mathematics

MDPI

Article

Multimode Representation of the Magnetic Field for the Analysis of the Nonlinear Behavior of Solar Activity as a Driver of Space Weather

Elena Popova [1], Anatoli I. Popov [2,*] and Roald Sagdeev [3]

[1] Centro de Investigación en Astronomía, Universidad Bernardo O'Higgins, Santiago 8370854, Chile; elena.popova@ubo.cl
[2] Institute of Solid State Physics, University of Latvia, LV-1063 Riga, Latvia
[3] Department of Physics, University of Maryland, College Park, MD 20742-4111, USA; rsagdeev@gmail.com
* Correspondence: popov@latnet.lv

Abstract: Estimating and predicting space weather is important to the space industry and space missions. The driver of space weather, especially near the Earth, is solar activity, the study of which is an important task. In particular, there is a direction of problems based on models of solar magnetic field generation that require research. In our work, we build a nonlinear dynamic system of equations that describes the behavior of the solar magnetic field harmonics based on the alpha-omega dynamo model. We found that, at the beginning of the magnetic field generation process, when the dynamo number significantly exceeds the threshold, the most rapidly growing waves are in the lead. Then, over time, these waves stop growing quite quickly. In this case, the initially slowly increasing harmonics of the magnetic field become the leaders, which then make the main contribution to the process of magnetic field generation.

Keywords: space weather; dynamic systems; multimode representation; solar activity; nonlinear system

MSC: 37M10; 76W05

Citation: Popova, E.; Popov, A.I.; Sagdeev, R. Multimode Representation of the Magnetic Field for the Analysis of the Nonlinear Behavior of Solar Activity as a Driver of Space Weather. *Mathematics* **2022**, *10*, 1655. https://doi.org/10.3390/math10101655

Received: 15 April 2022
Accepted: 10 May 2022
Published: 12 May 2022

1. Introduction

The term "space weather" came into wide use in the 1990s during a period of intense space exploration [1]. This term covers the most practically important aspects of the science of solar–terrestrial connections [2]. Space weather is concerned with the time-varying conditions within the Solar System, including solar wind, emphasizing the space surrounding the Earth, including conditions in the magnetosphere, ionosphere, thermosphere, and exosphere [3]. In a practical sense, space weather topics include, for example, issues of forecasting solar [4–12] and geomagnetic activity [13–17], studying the impact of solar factors on technical systems (radio interference, radiation conditions, etc.) [18–21]. The consequences of space weather conditions include effects on biological systems and people [2–27]. Thus, solar activity is the driver of space weather [2,28–31] and is of particular interest for research [32–34]. Solar activity is studied in many ways, with the help of observations (e.g., Big Bear Solar Observatory, Big Bear, CA, USA; Kitt Peak National Observatory, Tucson, AZ, USA; Solar Flare Telescope, Tokyo, Japan, etc.), round-the-clock monitoring (plenty of information here [35]), as well as theoretical analysis. Future missions are also planned, such as Lagrange (European Space Agency, Paris, France) [36], which envisions two spacecraft to be positioned at Lagrangian points L_1 and L_5.

Solar activity includes processes associated with the formation and decay of strong magnetic fields in the solar atmosphere. These fields are generated in the depths of the Sun (in the convective zone) and then float to the surface [37].

The generation of magnetic fields in the Sun is usually associated with the dynamo process, which is based on the combined action of the differential rotation of a celestial

body and a measure of violation of the reflective invariance of flows in the zone of magnetic field generation, the so-called hydrodynamic helicity. In the Parker dynamo kinematic model [38], the velocity field is considered to be given, and the generated magnetic field is considered in the form of traveling waves. The magnetic field is considered as two components: a toroidal (or azimuthal) field extended along the parallels and a poloidal field extended along the meridians. The toroidal magnetic field is obtained from the poloidal one under the action of differential rotation, located inside the convective zone of the Sun. The reverse process of the transformation of a toroidal magnetic field into a poloidal one is carried out as a result of a violation of the mirror symmetry of convection in a rotating body. The Coriolis force, when acting on rising and expanding (descending and contracting) vortices, leads to the predominance of right-handed vortices in the northern hemisphere (left-handed vortices in the southern hemisphere). A measure of violation of the reflection invariance of flows in the convective zone of the Sun is hydrodynamic helicity. The electromotive force resulting from the action of Faraday's electromagnetic induction, after averaging over the velocity fluctuations, acquires a component $\alpha\vec{B}$ parallel to the average magnetic field $\vec{B}$. It closes the self-excitation circuit in the Parker dynamo. To characterize generation sources in dynamo theory, it is customary to combine the amplitudes of the alpha effect and differential rotation into a dimensionless parameter—the dynamo number, which becomes the main control parameter in the dynamo equations.

Solar cyclic activity associated with the generation of a magnetic field in the convective zone of the Sun [38], according to observational data, has a complex structure: for example, 22-year, quasi-biennial, secular cycles (Gleisberg cycle), global minima that occur periodically every several hundred years [7,39–42]. In [43], the photometric data of the star HR 1099 for the years 1975–2006 were analyzed, and 2 activity cycles with a period of 15–16 years and 5.3 ± 0.1 years were identified.

It can be assumed that such data may indicate that several waves of magnetic activity can be generated in these celestial bodies, which can evolve in different ways over time. The properties of such a wave packet should be determined by the spatial configuration of the dynamo sources and the magnitude of the dynamo numbers.

In [44], it was shown that there is a class of exact analytical solutions in the problem of generating several independent dynamo waves using the example of a plane problem with two sources of generation. In such a problem, it was assumed that the distribution of differential rotation has the form of two narrow potential wells, the profile of which can be described by two delta functions, and the alpha effect does not depend on depth. It turned out that each of the waves in this case mainly interacts with its source, and its frequency depends on its physical parameters (dynamo number) and the degree of mutual overlap of the waves decreases with increasing distance between the sources.

Thus, two or more waves may appear if there are two or more "potential holes" (dynamo sources).

When the waves from such dynamo sources have close frequencies, beats can occur when they interact. Assumptions that this can lead to grand minima of solar activity were made in [45,46]. In [7] for two-layer and in [47] for three-layer media, $\alpha\Omega$-dynamo models with meridional matter flows were constructed, and the occurrence of global minima of solar magnetic activity and the Gleisberg cycle was simulated. In these models, the authors also tried to qualitatively reproduce the regimes of intense solar activity between long minima. Such variations in solar activity could be associated with small changes in the main parameters of the Sun, for example, meridional flows. However, this question is still open.

Several waves can also arise in the case of one potential well wide enough to accommodate several wavelengths (as a function of depth along the convective layer).

It can be assumed that, in this case, one cannot limit oneself to only one eigenfunction corresponding to the most rapidly growing solution due to the suppression of the alpha effect.

The purpose of this work is to show, using the example of a one-dimensional $\alpha\Omega$-dynamo model, how waves evolve in a nonlinear medium.

2. Main Equations

The system of $\alpha\Omega$-dynamo Parker equations [38] in the quasi-one-dimensional case has the following form:

$$\frac{\partial A}{\partial t} = R_\alpha \alpha B + \frac{\partial^2 A}{\partial \theta^2} \tag{1}$$

$$\frac{\partial B}{\partial t} = R_\omega \sin\theta \frac{\partial A}{\partial \theta} + \frac{\partial^2 B}{\partial \theta^2} \tag{2}$$

where the vector potential of the poloidal magnetic field A and the toroidal component B of the magnetic field are functions of latitude θ, measured from the pole, and time t. Dimensionless numbers R_α and R_ω, similar to the Reynolds number known in hydrodynamics, characterize the intensity of the α-effect and differential rotation, respectively ($D = R_\alpha R_\omega$). Usually, in solar dynamo problems, D is taken to be less than zero, and the modulus D is assumed in the analysis; therefore, in what follows, we will assume the modulus of D. Here, we use the simplest scheme for stabilizing the growth of the magnetic field, the so-called helicity suppression. Within the framework of this scheme, it is considered that:

$$\alpha = \alpha_0(\theta)/(1 + \xi^2 B^2) \approx \alpha_0(\theta)(1 - \xi^2 B^2), \tag{3}$$

where $\alpha_0(\theta)$ is the value of helicity in a non-magnetized medium, and $B_0 = \xi^{-1}$ is the magnetic field at which the alpha-effect is significantly suppressed. We use the simplest form for the alpha-effect $\alpha_0(\theta) = \cos\theta$, which satisfies the condition that it be equal to zero at the equator and also satisfies the condition that the alpha-effect is strongest at high latitudes (due to its dependence upon the Coriolis force). As boundary conditions, we use the conditions $A(0) = B(0) = A(\pi) = B(\pi) = 0$, which correspond to dipole symmetry. The choice of the factor in the second equation corresponds to a decrease in the length of the parallel near the pole. Curvature effects are omitted in the diffusion terms. It is assumed that the radial gradient of the angular velocity does not change with θ. For reasons of symmetry, Equations (1) and (2) can be considered only for one (northern) hemisphere with conditions of antisymmetry (dipole symmetry) or symmetry (quadrupole symmetry) at the equator. Since the solar magnetic field has a dipole symmetry, this case is considered in this model. In system (1) and (2), time and distances are measured in dimensionless units, which are introduced when constructing the dynamo number. In particular, the unit of time is not a year but the so-called diffusion time, during which a liquid particle passes through the convective zone under the action of turbulent diffusion. The estimate of diffusion time as a function of the parameters of the medium in which the field diffuses trough convective layer is $\frac{d^2}{\beta}$, where d is the thickness of the convective layer, and β is the coefficient of turbulent diffusion. The magnetic field is measured in units of the value at which the non-linear stabilization of the solution occurs (usually, it is assumed that there is an equipartition between the kinetic energy of turbulence and magnetic energy).

We will study systems (1) and (2) by expanding them into Fourier series with time-dependent coefficients. For the first time, such an approximation was proposed in [48] and developed in [49–55]. Note that dynamic systems are also used for other dynamo configurations, such as, for example, in [56], where the dynamic system was built for a disk dynamo system with three coupled conducting disks, and the interaction-induced time delay was taken into account in the dynamic control equations. Within the framework of this approximation, it is assumed that the excited magnetic field of a star or planet can be described by a suitably chosen dynamical system. The dynamo equations are projected onto a system of eigenfunctions for the problem of magnetic field damping in the absence of generation sources. The solution of the dynamo system is actually represented as a Fourier series with time-dependent unknown coefficients, which can be found from the

dynamic system for them obtained after substituting the chosen type of solution into the original dynamo system.

In [48–55], the solution was built on the basis of a small number of higher eigenfunctions (no more than three). However, when narrowing the basis of eigenfunctions (modes), it is very important not to go beyond the limits of applicability of this method when choosing large values of the dynamo number.

If the initially specified dynamo number significantly exceeds its threshold value (threshold of magnetic field generation), it is necessary to take into account a larger number of eigenfunctions (thus, their Fourier harmonics). If this condition is violated, the entire nonlinear picture of instability saturation will turn out to be incorrect. Depending on whether the dynamo number exceeds its threshold value, we estimate the minimum number of modes (harmonics) that must be taken into account on this basis. If the short-wavelength modes initially fall into the region of sufficiently strong attenuation due to magnetic turbulent diffusion, their contribution becomes negligible. Let a sufficiently large dynamo number D_0 be specified at the initial moment of time, and let us estimate the minimum number of modes that must be taken into account on the basis of eigenfunctions when solving the nonlinear dynamic problem of magnetic field growth and its nonlinear saturation. At large D_0, when the number of growing modes is sufficiently large ($n >> 1$), it is possible to apply the assumption of weak spatial inhomogeneity and find the local value of the growth rate of the dynamo wave. Let us substitute into the system of Equations (1) solutions in the form $A = \widetilde{A}\exp^{i(2n+1)\theta}\exp^{\omega t}$, $B = \widetilde{B}\exp^{i2n\theta}\exp^{\omega t}$, taking into account the dipole symmetry of the magnetic field. For $n >> 1$, it can be shown that if we put the average value $\sin\theta\cos\theta \approx 1/4$, then $Re\omega = \pm\frac{1}{\sqrt{2}}\sqrt{\frac{2nD}{4} - (2n)^2}$. The field generation condition is $\omega > 0$, hence $D > 8(2n)^3$. In a nonlinear balance, it is also necessary to take into account damped waves with slightly larger n. It is the nonlinear transfer of energy from unstable modes to dampened ones that ensures the establishment of nonlinear saturation. Then, when the dynamo number significantly exceeds the generation threshold, it is necessary to take into account the number of modes $n > \frac{1}{4}D^{1/3}$. Then, the applicability of the method, depending on the number of modes taken into account, will be limited to the following ranges of dynamo numbers: for $n = 2$, $D < 512$; $n = 3$, $D < 1728$; $n = 5$, $D < 8000$; and $n = 10$, $D < 64{,}000$. We note that in [51,53,55] the case $n = 2$ was considered, and the dynamo problem was also studied on regions of dynamo numbers that go beyond the region of applicability of the method (In [51] the region of dynamo numbers D was up to 1000, in [53] up to 3000, and work [55] is based on the study of the behavior of dynamo waves in the range D from 10^4 to 10^7).

In typical cases, as in the Sun and stars, the expected dynamo number is much higher than the instability threshold. High modes with a sufficiently large wave vector k become unstable, which requires a more complex multimode approach to the nonlinear problem. In addition, the original statement took into account that the alpha effect α and the differential rotation depend on θ, α is proportional to $\cos\theta$, and the differential rotation is proportional to $\sin\theta$ in the case when the angle is measured from the pole.

It can be shown that the amplitudes of the magnetic field at the saturation stage correspond with high accuracy to the complete compensation of the excess of the dynamo number over the threshold due to the nonlinear decrease in the α effect $D - D_{cr} = \delta\alpha_{nonlin}\Delta V/(\beta^2 k^2)$, where $\delta\alpha_{nonlin} = \alpha_0 B^2/B_0^2$, β is the coefficient of turbulent diffusion, and ΔV is the differential rotation jump at the thickness of the effective magnetic field generation layer.

To study the behavior of harmonics in our problem, consider the case $n = 10$, for which the dynamo number of the Sun is in the range of applicability of the method. We also took into account a larger number of harmonics and found that their contribution to the solution is negligible. The toroidal field B and the vector potential A can be represented as:

$$B(\theta, t) = \sum_{n=1}^{10} b_n(t)\sin(2n\theta) \quad (4)$$

$$A(\theta, t) = \sum_{n=1}^{10} a_n(t) \sin\left((2n+1)\theta\right) \quad (5)$$

Substituting the chosen type of solution into system (1) and (2), we obtain a dynamic system of 20 equations for unknown functions $a_n(t)$ and $b_n(t)$. Since this system turns out to be too cumbersome, we do not present it here.

3. Results

Figures 1 and 2 show the initial stage of generation of the solar magnetic field for different and identical, respectively, initial amplitudes of the toroidal magnetic field for a dynamo number exceeding the threshold value. Matlab was used to solve the dynamic system equations, and the calculation time was seconds for the selected time intervals, which are shown in the figures. The horizontal axis corresponds to time, and the vertical axis corresponds to the amplitude of the toroidal magnetic field. The magnetic field components are marked with numbers corresponding to the number n from relations (3) and (4). It can be seen from the figure that, over time, even at large initial values of the amplitude of the field of the shortest waves, only the longest wavelength harmonics remain. This is the result of a nonlinear decrease in the dynamo number during the establishment of the nonlinear dynamo stage, which is accompanied by the transition of short-wavelength modes from an unstable state to a damped one.

In the multimode model, with a large excess of criticality, over time, significant suppression of high modes occurs and the main contribution will be made by the fundamental (long-wavelength) modes. This can be considered the result of self-organized criticality. However, there will be "impurities" of higher modes in the vibration spectrum. The presence of such "impurities" may play a role in explaining some of the observations.

Figure 3 shows the regime of magnetic field generation in the form of oscillations, which are present in solar activity. The dynamo number is far from the threshold value and corresponds to the solar one. The horizontal axis corresponds to time, and the vertical axis corresponds to the amplitude of the toroidal magnetic field. The figure shows the 10 first harmonics of the field. The harmonic with the longest wavelength has a large amplitude and the number of this harmonic is marked with the number "1" in the figure. The tenth harmonic tends to zero. The nearest harmonics to the first one have a small non-zero amplitude due to the transfer of energy from the first harmonic to generate which amplitude of the dynamo number is sufficient.

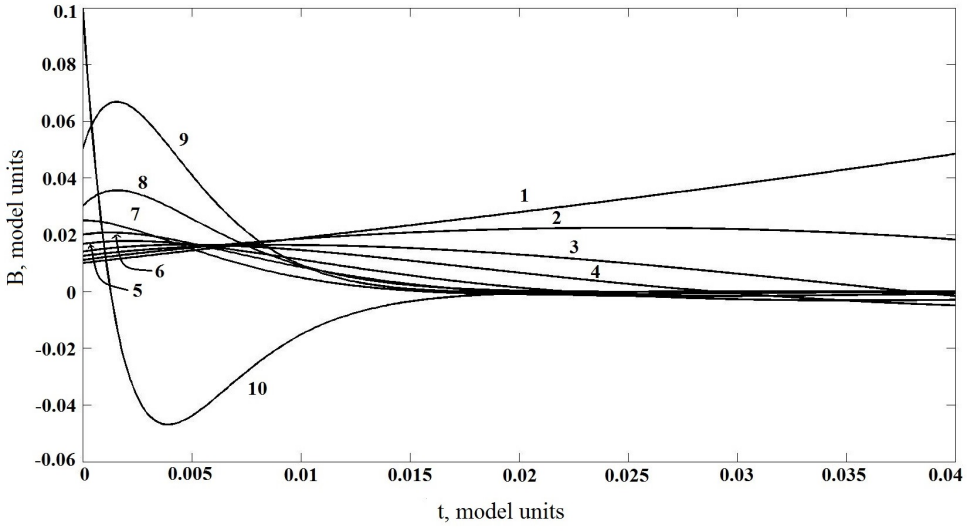

Figure 1. The dependence of the amplitude of the toroidal magnetic field on time for different initial amplitudes at the initial stage of generation.

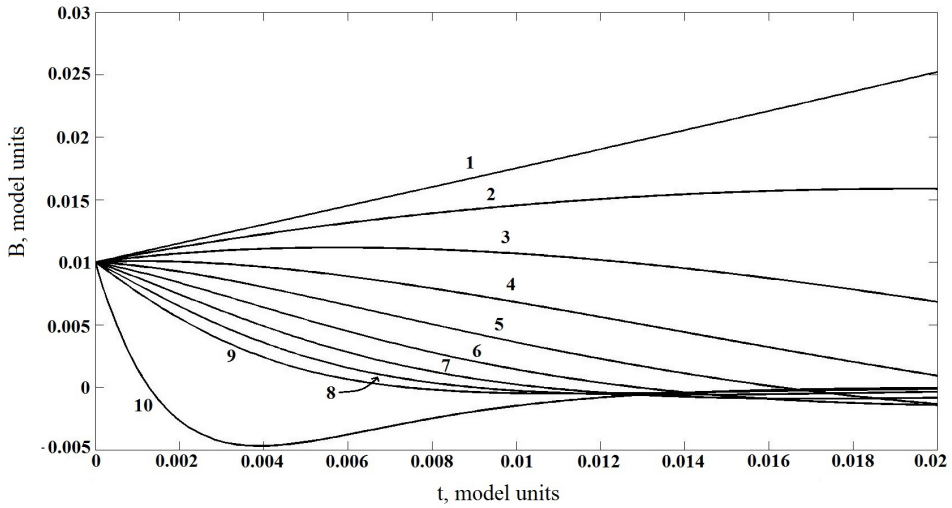

Figure 2. The dependence of the amplitude of the toroidal magnetic field on time for the same initial amplitudes at the initial stage of generation.

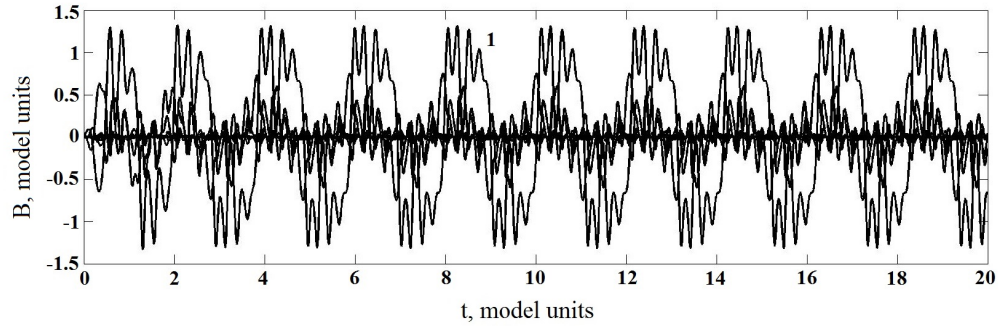

Figure 3. The dependence of the amplitude of the toroidal magnetic field on time for oscillatory regime.

Figure 4 shows a butterfly diagram for the case of Figure 3 (the regime of magnetic field generation in the form of oscillations). The horizontal axis corresponds to time, and the vertical axis corresponds to the latitude of the Sun, measured in degrees, where 0 corresponds to the equator and 90 degrees to the pole. The amplitude of the magnetic field is shown in the grayscale. The figure shows two patterns: one with a longer period and the other with a shorter one.

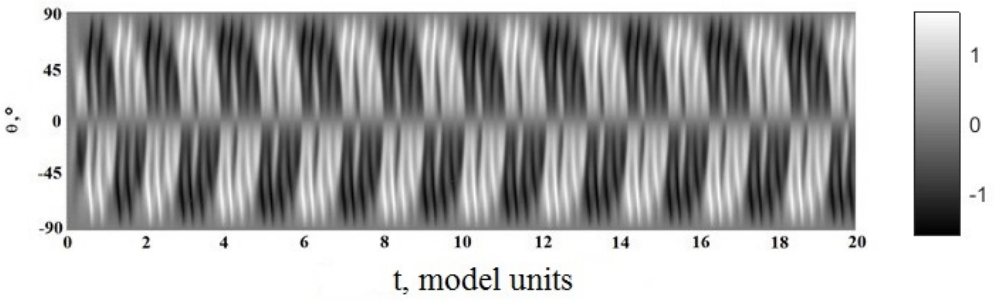

Figure 4. Butterfly diagram for oscillatory regime.

The pattern with a long period has the form of a wave going from the poles to the equator, has a duration of one diffusion unit, which corresponds to the observed butterfly diagram for the 11-year solar cycle, where the wave of the toroidal magnetic field also propagates from the poles to the equator. The pattern with a shorter period corresponds to

a quasi-biennial cycle, and the wave has the same direction as in the observational data: from the equator to the poles.

The resulting butterfly diagram has a qualitative difference from the picture of the observed configuration of sunspots, most of which are usually located near the equator. According to our model, we should observe sunspots distributed over all latitudes. This is because our study did not limit the alpha-effect to low latitudes (we assumed the alpha-effect dependence as $\cos\theta$, while θ was measured from the poles), so sunspot activity in our dynamo-model is not limited to low latitudes at the base of the convection zone. For a qualitative study of the time evolution of dynamo wave harmonics, this shortcoming does not play a significant role, since their latitude profile does not critically affect their time behavior for the simplest estimates.

Figure 5 shows dependence α-effect on time for case of Figures 3 and 4.

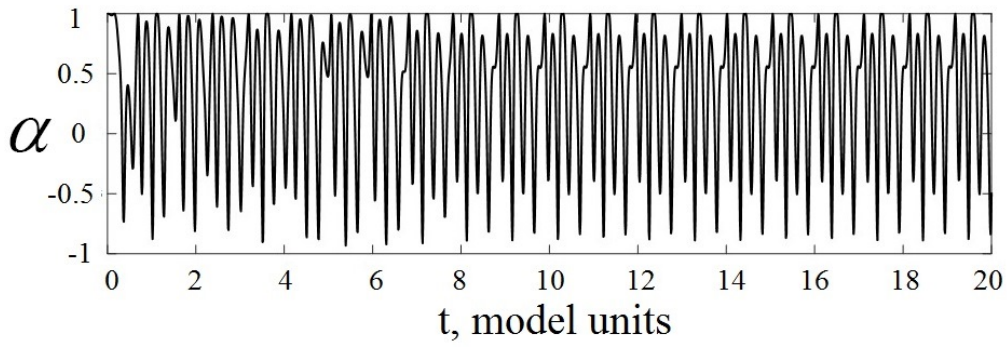

Figure 5. Dependence of α-effect on time.

From the results obtained, the following conclusion can be drawn. When the fastest growing solution enters the nonlinear stage and the alpha effect decreases, starting from some amplitudes, the wave stops growing; the neighboring harmonics, which initially grew slowly, catch up with the previous ones; and the fastest of them also begin to decay. Ultimately, the slowest growing waves come to the fore. A similar effect was noted in the works of A. Brandenburg [57–59], who said that several different modes can be excited before the saturation of the field generation. In the nonlinear mode, most of the modes are suppressed by the most dominant mode, and therefore, the nonlinearity has the effect of "self-cleaning" (nonlinear sweep). In [57–59], the simplest version of the dynamo in the box was considered when, in a rectangular potential well (a well as in quantum mechanics), there is no dependence on the coefficients of the equation on spatial coordinates. In our paper, we chose the latitude-dependent spatial distribution profiles for the alpha-effect and differential rotation to be solar-like. Thus, we solved the problem with a more complex profile, and the solution had to be sought in the form of irritation in the Fourier series. We have found how many terms in the expansion are sufficient to correctly describe the generation of the magnetic field.

Therefore, to simulate the generation of a magnetic field with dynamo numbers significantly exceeding the threshold for generating a magnetic field, one cannot limit oneself to only one (or even several) eigenfunctions corresponding to the most rapidly growing solution. Such a wave eventually stops growing, leaves the game, and its contribution to the process of magnetic field generation becomes insignificant. In other words, the dynamo number decreases in the process of reaching the nonlinear saturation mode, and the modes at the beginning of the process, which were the most unstable, would formally become damped so that their amplitudes are eventually maintained by the nonlinear energy transfer from large-scale waves.

4. Conclusions

We built the nonlinear dynamic system of equations that describes the behavior of the solar magnetic field harmonics based on the alpha-omega dynamo model. At the beginning

of the magnetic field generation process, when the dynamo number significantly exceeds the threshold, the most rapidly growing waves are in the lead. Then, over time, these waves stop growing quite quickly. In this case, the initially slowly increasing harmonics of the magnetic field become the leaders, which then make the main contribution to the process of magnetic field generation. This can be considered the result of self-organized criticality. "Impurities" of higher modes can present in the vibration spectrum. It is due to the nearest harmonics to the first one have a small non-zero amplitude due to the transfer of energy from the first harmonic to generate which the amplitude of the dynamo number is sufficient. The presence of such "impurities" may play a role in explaining the presence of quasi-biennial oscillations in solar cycle.

The method used to study the behavior of the waves of the solar magnetic field and the dynamo model has a number of limitations and simplifications. For example, the latitudinal profile of the alpha-effect is not zero at high latitudes, and this leads to a qualitative difference between the theoretical and observed butterfly diagrams discussed above. Although, it "does the right thing", alpha tends to zero as magnetic field B starts to exceed B_0 and is widely used in solar dynamo models, it remains an extreme oversimplification of the complex interaction between flow and field that characterizes MHD turbulence.

Also for the latitudinal profile of the differential rotation, we use the simplest form [58], but for our task, it is quite adequate.

To further develop the proposed model, more realistic differential rotation and alpha-effect profiles can be used, as well as meridional flows can be added. Questions of time variation of solar activity from global minima to intense regular activity remain open, in addition, the question of modeling the occurrence of explosive processes associated with the generation of a magnetic field—superflares are still open, too.

Despite the existence of complex and much more realistic models [58,60] that require lengthy calculations on supercomputers, our model allows us to give simple qualitative estimates of the field behavior without resorting to large computational resources. Such an approach can be useful in the initial testing of physical assumptions, on the basis of which more complex and realistic models can then be built to more correctly reproduce the processes under consideration.

Author Contributions: E.P. methodology, investigation, main ideas, writing—original draft preparation, writing—review and editing; A.I.P. consultation, writing—review and editing; R.S. methodology, investigation, main ideas, writing—review and editing. All authors have read and agreed to the published version of the manuscript.

Funding: ISSP UL as the Center of Excellence is supported through the Framework Program for European universities Union Horizon 2020, H2020-WIDESPREAD-01-2016-2017-TeamingPhase2 under Grant Agreement No. 739508, CAMART2 project; Internal Foundation of University of Maryland.

Institutional Review Board Statement: Not applicable.

Informed Consent Statement: Not applicable.

Data Availability Statement: Not applicable.

Acknowledgments: A.I.P would like to thank the Institute of Solid State Physics, University of Latvia (ISSP UL).

Conflicts of Interest: The authors declare no conflict of interest.

References

1. Cade, W.B., III; Chan-Park, C. The origin of "space weather". *Space Weather* **2015**, *13*, 99–103. [CrossRef]
2. Buzulukova, N. (Ed.) *Extreme Events in Geospace: Origins, Predictability, and Consequences*; Elsevier: Cambrige, MA, USA, 2017.
3. Poppe, B.B.; Jorden, K.P. *Sentinels of the Sun: Forecasting Space Weather*; Big Earth Publishing: Boulder, CO, USA, 2006.
4. Berghmans, D.; Van der Linden, R.A.M.; Vanlommel, P.; Warnant, R.; Zhukov, A.; Robbrecht, E.; Clette, F.; Podladchikova, O.; Nicula, B.; Hochedez, J.F.; et al. Solar activity: Nowcasting and forecasting at the SIDC. *Ann. Geophys.* **2005**, *23*, 3115–3128. [CrossRef]

5. Miteva, R.; Samwel, S.W. M-Class Solar Flares in Solar Cycles 23 and 24: Properties and Space Weather Relevance. *Universe* **2022**, *8*, 39. [CrossRef]
6. Zhang, W.; Zhao, X.; Feng, X.; Liu, C.A.; Xiang, N.; Li, Z.; Lu, W. Predicting the Daily 10.7-cm Solar Radio Flux Using the Long Short-Term Memory Method. *Universe* **2022**, *8*, 30. [CrossRef]
7. Zharkova, V.V.; Shepherd, S.J.; Popova, E.; Zharkov, S.I. Heartbeat of the Sun from Principal Component Analysis and prediction of solar activity on a millenium timescale. *Sci. Rep.* **2015**, *5*, 15689. [CrossRef]
8. Tuohy, A.; Zack, J.; Haupt, S.E.; Sharp, J.; Ahlstrom, M.; Dise, S.; Grimit, E.; Mohrlen, C.; Lange, M.; Casado, M.G.; et al. Solar forecasting: Methods, challenges, and performance. *IEEE Power Energy Mag.* **2015**, *13*, 50–59. [CrossRef]
9. Voyant, C.; Notton, G.; Kalogirou, S.; Nivet, M.L.; Paoli, C.; Motte, F.; Fouilloy, A. Machine learning methods for solar radiation forecasting: A review. *Renew. Energy* **2017**, *105*, 569–582. [CrossRef]
10. Okoh, D.I.; Seemala, G.K.; Rabiu, A.B.; Uwamahoro, J.; Habarulema, J.B.; Aggarwal, M. A Hybrid Regression-Neural Network (HR-NN) method for forecasting the solar activity. *Space Weather* **2018**, *16*, 1424–1436. [CrossRef]
11. Colak, T.; Qahwaji, R. Automated solar activity prediction: A hybrid computer platform using machine learning and solar imaging for automated prediction of solar flares. *Space Weather* **2009**, *7*, 6. [CrossRef]
12. Reikard, G. Forecasting long-term solar activity with time series models: Some cautionary findings. *J. Atmos. Sol.-Terr. Phys.* **2020**, *211*, 105465. [CrossRef]
13. Joselyn, J.A. Geomagnetic activity forecasting: The state of the art. *Rev. Geophys.* **1995**, *33*, 383–401. [CrossRef]
14. Wei, H.L.; Zhu, D.Q.; Billings, S.A.; Balikhin, M.A. Forecasting the geomagnetic activity of the Dst index using multiscale radial basis function networks. *Adv. Space Res.* **2007**, *40*, 1863–1870. [CrossRef]
15. Hernandez, J.V.; Tajima, T.; Horton, W. Neural net forecasting for geomagnetic activity. *Geophys. Res. Lett.* **1993**, *20*, 2707–2710. [CrossRef]
16. Jackson, B.V.; Yu, H.S.; Buffington, A.; Hick, P.P.; Tokumaru, M.; Fujiki, K.; Kim, J.; Yun, J. A daily determination of BZ using the Russell-McPherron effect to forecast geomagnetic activity. *Space Weather* **2019**, *17*, 639–652. [CrossRef]
17. Haines, C.; Owens, M.J.; Barnard, L.; Lockwood, M.; Ruffenach, A.; Boykin, K.; McGranaghan, R. Forecasting Occurrence and Intensity of Geomagnetic Activity With Pattern-Matching Approaches. *Space Weather* **2021**, *19*, e2020SW002624. [CrossRef]
18. Ulsrud, K.; Winther, T.; Palit, D.; Rohracher, H.; S.; Sandgren, J. The Solar Transitions research on solar mini-grids in India: Learning from local cases of innovative socio-technical systems. *Energy Sustain. Dev.* **2011**, *15*, 293–303. [CrossRef]
19. Wik, M.; Pirjola, R.; Lundstedt, H.; Viljanen, A.; Wintoft, P.; Pulkkinen, A. April. Space weather events in July 1982 and October 2003 and the effects of geomagnetically induced currents on Swedish technical systems. *Ann. Geophys.* **2009**, *27*, 1775–1787. [CrossRef]
20. Haines, O.D.; Kennewell, J.; Lynch, M. Solar radio burst statistics and implications for space weather effects. *Space Weather* **2017**, *15*, 1511–1522.
21. Nwankwo, V.U.; Jibiri, N.N.; Kio, M.T. The impact of space radiation environment on satellites operation in near-Earth space. In *Satellites Missions and Technologies for Geosciences*; InTechOpen Publishing: London, UK, 2020.
22. Senatore, G.; Mastroleo, F.; Leys, N.; Mauriello, G. Effect of microgravity and space radiation on microbes. *Future Microbiol.* **2018**, *13*, 831–847. [CrossRef]
23. Miura, K.; Olsen, C.M.; Rea, S.; Marsden, J.; Green, A.C. Do airline pilots and cabin crew have raised risks of melanoma and other skin cancers? Systematic review and meta-analysis. *Br. J. Dermatol.* **2019**, *181*, 55–64. [CrossRef]
24. Dreger, S.; Wollschläger, D.; Schafft, T.; Hammer, G.P.; Blettner, M.; Zeeb, H. Cohort study of occupational cosmic radiation dose and cancer mortality in German aircrew, 1960–2014. *Occup. Environ. Med.* **2020**, *77*, 285–291. [CrossRef] [PubMed]
25. Townsend, L.W. Space Radiation Environment. In *Handbook of Bioastronautics*; Springer: Berlin/Heidelberg, Germany, 2021; pp. 335–346.
26. Stewart, G. Omaha Field—A Magnetostatic Cosmic Radiation Shield for a Crewed Mars Facility. *Terraforming Mars* **2021**, *2021*, 281–296.
27. Lim, M.K. Cosmic rays: Are air crew at risk? *Occup. Environ. Med.* **2002**, *59*, 428–432. [CrossRef] [PubMed]
28. Kuznetsov, N.V.; Popova, H.; Panasyuk, M.I. Empirical model of long-time variations of galactic cosmic ray particle fluxes. *J. Geophys. Res. Space Phys.* **2017**, *122*, 1463–1472. [CrossRef]
29. Kamide, Y.; Kusano, K. No major solar flares but the largest geomagnetic storm in the present solar cycle. *Space Weather* **2015**, *13*, 365–367. [CrossRef]
30. Tang, J.; Li, Y.; Yang, D.; Ding, M. An Approach for Predicting Global Ionospheric TEC Using Machine Learning. *Remote Sens.* **2022**, *14*, 1585. [CrossRef]
31. Schmolter, E.; Berdermann, J. Predicting the Effects of Solar Storms on the Ionosphere Based on a Comparison of Real-Time Solar Wind Data with the Best-Fitting Historical Storm Event. *Atmosphere* **2021**, *12*, 1684. [CrossRef]
32. Zendehboudi, A.; Baseer, M.A.; Saidur, R. Application of support vector machine models for forecasting solar and wind energy resources: A review. *J. Clean. Prod.* **2018**, *199*, 272–285. [CrossRef]
33. Inman, R.H.; Pedro, H.T.; Coimbra, C.F. Solar forecasting methods for renewable energy integration. *Prog. Energy Combust. Sci.* **2013**, *39*, 535–576. [CrossRef]
34. Perez, R.; Moore, K.; Wilcox, S.; Renné, D.; Zelenka, A. Forecasting solar radiation–Preliminary evaluation of an approach based upon the national forecast database. *Sol. Energy* **2007**, *81*, 809–812. [CrossRef]

35. Space Weather Service Network of European Space Agency. Available online: https://swe.ssa.esa.int/current-space-weather (accessed on 14 April 2022).
36. Kraft, S.; Puschmann, K.G.; Luntama, J.P. Remote sensing optical instrumentation for enhanced space weather monitoring from the L1 and L5 Lagrange points. In Proceedings of the International Conference on Space Optics—ICSO 2016, Biarritz, France, 18–21 October 2016; Volume 10562, p. 105620F.
37. Balogh, A.; Hudson, H.; Petrovay, K.; Steiger, R. (Eds.) *The Solar Activity Cycle: Physical Causes and Consequences*; Springer: Berlin/Heidelberg, Germany, 2015; Volume 53.
38. Parker, E.N. Hydrodynamic dynamo models. *Astrophys. J.* **1955**, *122*, 293–314. [CrossRef]
39. Gleissberg, W. The eighty-year cycle in auroral frequency numbers. *J. Brit. Astr. Assoc.* **1965**, *75*, 227–231.
40. Schove, D.J. *Sunspot Cycles*; Benchmark Papers in Geology; Hutchinson Ross Publishing Co.: Stroudsburg, PA, USA, 1983; 410p.
41. Sakurai, K. Quasi-biennial variation of the solar neutrino flux and solar activity. *Nature* **1979**, *278*, 146–148. [CrossRef]
42. Deng, L.H.; Fei, Y.; Deng, H.; Mei, Y.; Wang, F. Spatial distribution of quasi-biennial oscillations in high-latitude solar activity. *Mon. Not. R. Astron. Soc.* **2020**, *494*, 4930–4938. [CrossRef]
43. Berdyugina, S.V.; Henry, G.W. Butterfly diagram and activity cycles in HR 1099. *Astrophys. J.* **2007**, *659*, L157–L160. [CrossRef]
44. Popova, E.P. Generation of magnetic field waves in celestial bodies by spatially separated sources. *Dokl. Phys.* **2017**, *62*, 371–373. [CrossRef]
45. Boyer, D.W.; Levy, E.H. Multiple periodicities in the solar magnetic field-Possible origin in a multiple-mode solar dynamo. *Astrophys. J.* **1992**, *396*, 340–350. [CrossRef]
46. Merzlyakov, V.L. Solar activity as a result of two-wave magnetic flux generation. *Sol. Phys.* **1997**, *170*, 425–435. [CrossRef]
47. Popova, E.; Zharkova, V.; Shepherd, S.; Zharkov, S. On a role of quadruple component of magnetic field in defining solar activity in grand cycles. *J. Atmos. Sol. Terr. Phys.* **2018**, *176*, 61–68. [CrossRef]
48. Ruzmaikin, A.A. Solar cycle as strange attractor. *Comm. Astrophys.* **1981**, *9*, 85–93.
49. Kitiashvili, I.; Kosovichev, A.G. Application of Data Assimilation Method for Predicting Solar Cycles. *Astrophys. J.* **2008**, *688*, L49. [CrossRef]
50. Kitiashvili, I.; Kosovichev, A.G. Nonlinear dynamical modeling of solar cycles using dynamo formulation with turbulent magnetic helicity. *Geophys. Astrophys. Fluid Dyn.* **2009**, *103*, 53–68. [CrossRef]
51. Nefedov, S.; Sokoloff, D. Parker's dynamo as specific behavior of a dynamical system. *Astron. Rep.* **2010**, *54*, 247–253. [CrossRef]
52. Popova, H. Double Magnetic Solar Cycle and Dynamical Systems. *Magnetohydrodynamics* **2013**, *49*, 59–67. [CrossRef]
53. Sobko, G.; Zadkov, V.; Sokoloff, D.; Trukhin, V. Geomagnetic reversals in a simple geodynamo model. *Geomagn. Aeron.* **2012**, *52*, 254–260. [CrossRef]
54. Sokoloff, D.; Nefedov, S. Low-mode approximation in the problem of star dynamo. *Numer. Methods Program.* **2007**, *8*, 195–204.
55. Tarbeeva, S.M.; Sokoloff, D.D. Oppositely directed waves of stellar activity in simple dynamo models. *Astron. Rep.* **2016**, *60*, 682–686. [CrossRef]
56. Deng, S.; Ji, J.; Wen, G.; Xu, H. A comparative study of the dynamics of a three-disk dynamo system with and without time delay. *Appl. Math. Comput.* **2021**, *399*, 126016. [CrossRef]
57. Brandenburg, A. The Inverse cascade and nonlinear alpha-effect in simulations of isotropic helical hydromagnetic turbulence. *Astrophys. J.* **2001**, *550*, 824–840. [CrossRef]
58. Brandenburg, A. Astrophysical magnetic fields and nonlinear dynamo theory. *Phys. Rep.* **2005**, *417*, 1–209. [CrossRef]
59. Brandenburg, A.; Subramanian, K. Large scale dynamos with ambipolar diffusion nonlinearity. *Astron. Astrophys.* **2000**, *361*, 33–36.
60. Brandenburg, A. Advances in mean-field dynamo theory and applications to astrophysical turbulence. *J. Plasma Phys.* **2018**, *84*, 735840404. [CrossRef]